Physica B 404 (2009) 4216–4220

Contents lists available at ScienceDirect

Physica B

journal homepage: www.elsevier.com/locate/physb

The changes in the electronic structure of B2 FeAl alloy with a Fe antisite and absorbed hydrogen

E.A. Gonzalez, P.V. Jasen, R. Luna, P. Bechthold, A. Juan, G. Brizuela *

Departamento de Física, Universidad Nacional del Sur, Av. Alem 1253, Bahía Blanca (8000), Argentina

ARTICLE INFO

Article history:
Received 16 January 2009
Accepted 3 August 2009

Keywords:
Alloys
Ab-initio calculations
Defects
Electronic structure

ABSTRACT

The electronic structure and bonding in a B2 FeAl alloy with and without hydrogen interaction with a Fe antisite were computed using a density functional theoretical method. The hydrogen absorption turns out to be a favorable process. The hydrogen was found close to an octahedral site where one of its Al capped is replaced by a Fe antisite. The Fe–H distance is of 1.45 Å same as the Al–H distance.

The density of states (DOS) curves show several peaks below the d metal band which is made up mostly of hydrogen based states ($>50\%$ H_{1s}) while the metal contribution in this region includes mainly s and p orbitals.

An electron transfer of nearby $0.21e^-$ comes from the metal to the H. The overlap population values reveal metal–metal bond breaking, the intermetallic bond being the most affected. The H bond mainly with the Al atom and the reported Fe–H overlap population is much lower than that corresponding to FePd alloys and BCC Fe. The changes in the overlap population show the Fe–Al bond is weakened nearly 41.5% after H absorption, while the Fe–Fe bond is only weakened 34.5%. H also develops a stronger bond with the Al atoms. The main bond is developed with Al being twice stronger than Fe–H.

1. Introduction

The chemical bonding in iron aluminides has attracted attention over the last years. Yield strength anomaly, vacancy hardening, and the effect of alloying elements on hydrogen embrittlement have stimulated interest in this subject. A clear understanding of the mechanical, electrical, and thermodynamic properties of alloyed iron aluminides require the study of the features of metal–metal bonding in these alloys, doped by other elements and with defects present [1].

Both chemical bonding and site preference occupation of transition metal (TM) in Fe–Al result from chemical properties of the TM, which determine the atomic coordination according to the Pauling concept [2].

Vacancy and antisite defect energies are important in the accommodation of stoichiometry deviations. It has been observed in FeAl and NiAl [3,4] that Al-deficient compounds present only antisite defects while constitutional vacancies accommodate the variation from stoichiometry in Al-rich compounds. In order to accommodate deviation from stoichiometry, either two vacancies or one antisite could occur. Using the energy values obtained by embedded atom potentials, Vailhe and Farkas [5] predict antisite defects on both sides of the stoichiometric composition. In the case of an Al-rich compound, the predictions of the potentials did not agree with the experimental observations of Xiao et al. [3] and Baker and Munroe [4], but agree with the more recent experimental observation of Hosada et al. [6].

B2-type FeAl is known to be an intermetallic compound that generates a large number of thermal vacancies at high temperature and retains them in supersaturation through conventional cooling processes [7]. The vacancy concentration should approach several percent near its melting point, which is two times higher than that of pure metals and disordered alloys. The primary reasons for this unique vacancy phenomenon are the properties of low vacancy formation enthalpy and high vacancy formation entropy in B2-type FeAl [8].

There are an interesting number of theoretical studies on intermetallic alloys [9–19]. Zou and Fu have shown that the dominant factor for early TM aluminides is the directional bonding between the d orbital of TM atoms, whereas for late TM aluminides, charge transfer and hybridization between Al sp and TM d states play more important roles in the bonding [10].

Theoretical calculations have been performed in Fe aluminides by Schott and Fänhle [12] and by Bogner et al. [20]. The electronic structure of iron aluminides has also been computed using clusters and extended structures of variable Al composition [13–16]. Recently, density functional theory (DFT) in the local density approximation with the Hubard Hamiltonian (LDA+U) [17] and

* Corresponding author. Tel./fax: +54 291 4595142.
E-mail address: brizuela@criba.edu.ar (G. Brizuela).

0921-4526/$ - see front matter © 2009 Elsevier B.V. All rights reserved.
doi:10.1016/j.physb.2009.08.020

accurate tight-binding (TB) parameterization of LDA schemes yield a non-magnetic ground state for B2 FeAl [17,18]. The difficulties to reproduce experimental ground states for FeAl and Fe_3Al have been pointed out by Lechermann et al. [19]. DFT has also been used to study the behavior of single defects in B2-FeAl-vacancies, as well as boron, carbon, nitrogen, and oxygen substituting for Fe or Al atoms [21–23]. The environmental embrittlement in FeAl aluminides has been reviewed by Liu et al. [22].

The aim of the present is to evaluate the changes in the metal–metal bonding when a Fe antisite is present and its interaction with hydrogen as an impurity.

2. Computational method

Gradient-corrected density functional theory (GC-DFT) calculations were performed on a supercell containing 108 atomic sites in a cubic lattice (B2-phase) to model bulk FeAl, with a $4\times4\times4$ reciprocal space grid in the supercell Brillouin zone. We used the Amsterdam Density Functional 2000 package (ADF-BAND2000) [24]. The molecular orbitals were represented as linear combinations of Slater functions. The gradient correction of the Becke [25] approximation for the exchange energy functional and the B3LYP [26] approximation for the correlation functional were employed.

In order to increase the computational efficiency, the innermost atomic shells of electrons are kept frozen for every atom except hydrogen, since the internal electrons do not contribute significantly to the bonding. We have used a triple-zeta basis set (this means three Slater-type functions for each atomic valence orbital occupied) with polarization functions to express the atomic orbitals of Fe and Al. The basis set of Fe consisted of 3p, 3d and 4s orbitals and for Al 3s and 3p. With this set we obtained a magnetic moment of 2.26μB for BCC Fe, which compares very well with the experimental value of 2.20μB.

To understand the Fe–Al–H interactions we used the concept of density of states (DOS) and overlap population density of states (OPDOS). The DOS curve is a plot of the number of orbitals as a function of the energy. The integral of the DOS curve over an energy interval gives the number of one-electron states in that interval; the integral up to the Fermi level (E_F) gives the total number of occupied molecular orbitals. If the DOS is weighed with the overlap population between two atoms the overlap population density of states OPDOS is obtained. The integration of the OPDOS curve up to E_F gives the total overlap population of the specified bond orbital and it is a measure of the bond strength. If an orbital at certain energy is strongly bonding between two atoms the overlap population is strongly positive and OPDOS curve will be large and positive around that energy. Similarly, OPDOS negative around a certain energy corresponds to antibonding interactions.

The absorption energy was computed as the difference ΔE between the Fe–Al–H composite system when the H atom is absorbed at its minima location geometry and when it is far away from the Fe–Al alloy.

3. Crystal and defect structure

The B2 FeAl phase has ClCs structure with a lattice parameter $a_0 = 2.90$ Å [9]. The crystal structure is shown in Fig. 1a. The B2 FeAl structure has three types of interstitial sites, one tetrahedral (T) and two octahedral (O1, O2). All tetrahedral are equivalent with the same chemical environment around the site. The O2 is an octahedral formed by four iron atoms in its base capped with two aluminum atoms while the O1 has four aluminum atoms in its base capped with two iron atoms. We have considered an Al vacancy (V_{Al}) and Fe antisites (Fe_{Al}) separately. The Fe vacancies are the most stable while the Al vacancies cannot survive because they quickly transform into Fe antisites. We only present some V_{Al} results.

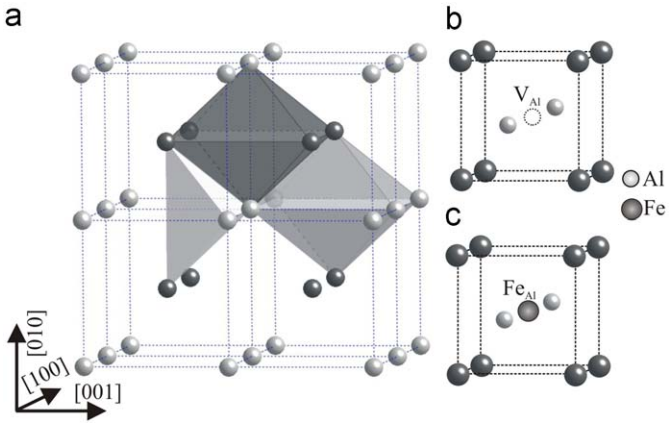

Fig. 1. Crystal structure of the B2 FeAl alloy (a). Schematic view of the Al vacancy frame (b). Schematic view of the Fe antisite frame (c).

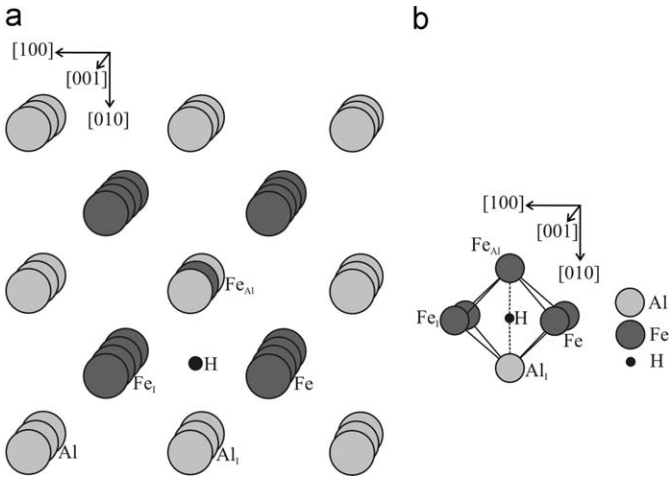

Fig. 2. Schematic view of the B2 FeAl+Fe_{Al} cell after H absorption (a). Schematic view of the frame H location (b). The small black circle indicates the energetic minima for H.

The vacancy was constructed removing the Al atom from the center of the cell. The Fe antisite was the next step of study and was created replacing the vacant site for a Fe atom.

To study the absorption of H we mapped the energy surfaces with 0.01 Å steps in the central region of the cell with cuts perpendicular to the (0 0 1) planes. Fig. 2 shows the final location of the H atom. Fig. 2b shows the chemical environment for H absorption.

4. Results and discussion

The total DOS for the perfect B2 FeAl structure is similar to that reported previously [9–18,27–34]. First principles calculations have mentioned the formation of a pseudo-band gap at the top of the 3d band [33,35]. The d bandwidth is 3.6 eV, which corresponds to the extension of the Fe states while Al based states contribute much less, showing several peaks. Near the Fermi level there is also a peak centered at −10.2 eV somewhat dispersed and corresponds to Al p states (see Fig. 3b). Similar results for Al and Fe orbital projected DOS were reported by Reddy et al. [13].

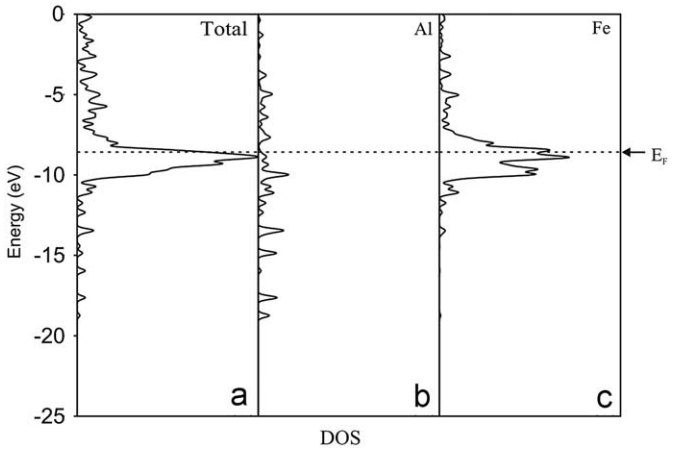

Fig. 3. Total DOS curves for the B2 FeAl–V_{Al} alloy (a); projected DOS in an Al atom (b); and in a Fe atom (c).

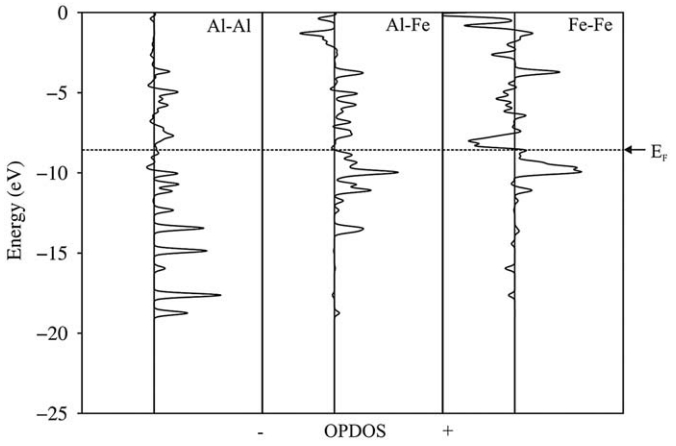

Fig. 4. OPDOS curves of the B2 FeAl–V_{Al} alloy: Al–Al first neighbors (a), Al–Fe (b), and Fe–Fe (c).

The Al orbital composition is $s^{1.05}$ $p^{1.20}$ $d^{0.00}$. The electronic charge on Al is 70% lower of that on the Fe atoms [36]. The importance of Al to TM charge transfer and the filling of the d band require that a late TM atom has as many Al atoms as its nearest neighbors as possible to facilitate the charge transfer and bonding hybridization [10,20]. Several authors have mentioned a strong d state [20,33,37].

Regarding the bonding, the OPDOS curves in Fig. 4 show almost all bonding contributions. Reddy et al. mentioned that the conduction band approaches very close to the Fermi level and is mainly composed of hybridized Al sp–Fe d levels [16]. In Table 1, the valence orbital occupations, overlap populations, and distances are summarized.

When a vacancy is introduced into the model, the total DOS curve for the complete system (Fig. 3a) looks similar to that of the cell without a vacancy. The introduction of an Al vacancy makes the all metal–metal bond stronger than in the perfect case (see Table 1, ΔOP for all metals increases when compared to the perfect alloy). This effect has been discussed in detail by Juan and Hoffmann [38]. Comparing to the corresponding perfect alloy the bonding vacancy states are also less bonding and the antibonding states are less antibonding. For the bulk most all antibonding states are filled. As an antibonding level is in fact more antibonding than the corresponding bonding level is bonding, the loss of antibonding character dominates close to the vacancy (see Table 1) causing an increase in the metal–metal OP.

Table 1
Electronic density, overlap population, charge, and distances for the B2 FeAl perfect, the B2 FeAl–V_{Al}, the B2 FeAl–Fe_{Al}, and B2 FeAl–Fe_{Al} after H absorption alloy.

Structure	Electronic density			Bond type	OP	$\Delta OP\%$[a]	Distances (Å)
	s	p	d				
FeAl–V_{Al}							
Fe_I	0.44	0.11	6.50	Fe_I–Fe		26.4	2.904
Al_I	1.07	1.23	0.00	Al_I–Al		2.3	2.904
				Al_I–Fe_I		27.0	2.515
FeAl–Fe_{Al}							
Fe_I	0.44	0.09	6.24	Fe_I–Fe		−2.7	2.904
Al_I	1.07	1.22	0.00	Al_I–Al		2.3	2.904
				Al_I–Fe_I		14.5	2.515
Fe_{Al}	0.60	0.09	4.87	Al_I–Fe_{Al}		−54.4	2.904
				Fe_I–Fe_{Al}		−81.3	2.515
FeAl–Fe_{Al}+H							
Fe_I	0.41	0.06	6.14	Fe_I–Fe		−34.5	2.904
Al_I	0.98	1.19	0.00	Al_I–Al		−3.2	2.904
				Al_I–Fe_I		−41.5	2.515
Fe_{Al}	0.53	0.07	6.44	Al_I–Fe_{Al}		–[b]	2.904
				Fe_I–Fe_{Al}		−44.6	2.515
H	1.21	0.00	0.00	Fe_I–H	0.046		2.044
				Al_I–H	0.510		1.450
				Fe_{Al}–H	0.280		1.450

[a] ΔOP%: Overlap population percentage change computed referring to B2 FeAl pure [32].
[b] H locates between these two atoms, so there is no possible bonding in this case.

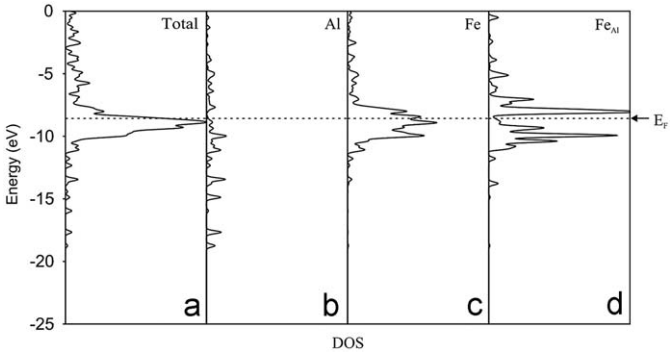

Fig. 5. Total DOS curves for the B2 FeAl–Fe_{Al} alloy (a); projected DOS in an Al atom (b), in a Fe atom (c), and in the Fe antisite (d).

In the case of antisite occupancy, the Fe_I–Fe_{Al} increases because its distance is lower than in the perfect lattice, so higher overlap is possible as revealed in the OP values. The computed effective formation energies are 3.50 eV for the vacancy and 1.03 eV for the Fe antisite. These values are in good agreement with that reported by Fähnle et al. [39].

As mentioned by Kellou et al. [21], a single Fe antisite has a lower energy than an Al antisite. Fig. 5 shows the DOS of Fe antisite in FeAl. The Fe antisite projected DOS (see Fig. 5d) shows a strong decrease in the density close to E_F. Similar results have been reported by Kulikov et al. [36] when considering a Fe at the central antisite.

The Al–Al OP does not change with Fe at the antisite (see Fig. 6 and Table 1). The OPDOS curves for the Fe–Fe present some antibonding at −17 eV; however, the total effect is positive increasing a 14.5%. The Fe–Fe antisite OP increases 129% while the distance decreases −13.4%.

The H absorption is a favorable process. The final location is shown in Fig. 2. It corresponds to and octahedral interstitial site

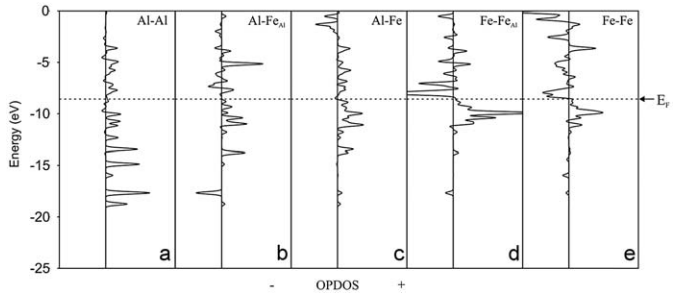

Fig. 6. OPDOS curves of the B2 FeAl–Fe$_{Al}$ alloy: Al–Al (a), Al–Fe$_{Al}$ (b), Al–Fe (c), Fe–Fe$_{Al}$ (d), and Fe–Fe (e) bonds.

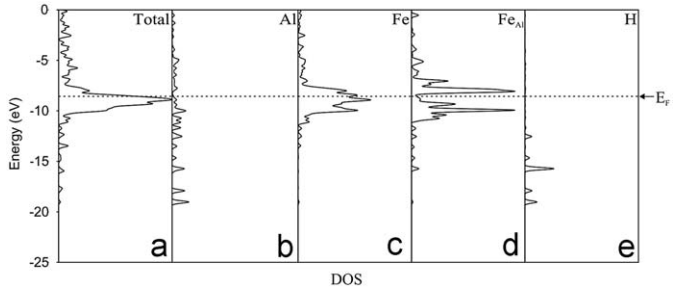

Fig. 7. Total DOS curves for the B2 FeAl–Fe$_{Al}$ alloy after H absorption (a); projected DOS in an Al atom (b), in a Fe atom (c), in the Fe antisite (d), and in the H atom (e).

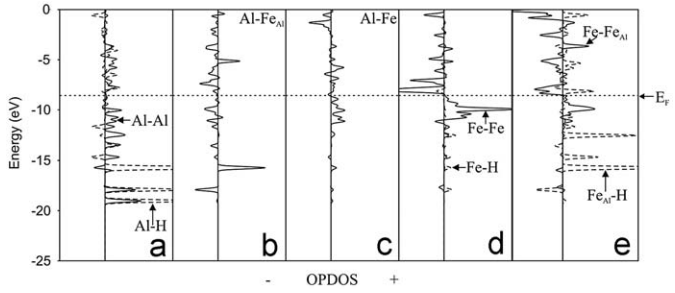

Fig. 8. OPDOS curves of the B2 FeAl–Fe$_{Al}$ alloy after H absorption: Al–Al and Al–H (dotted line) (a), Al–Fe$_{Al}$ (b), Al–Fe (c), Fe–Fe and Fe–H (dotted line) (d), and Fe–Fe$_{Al}$ and Fe$_{Al}$–H (dotted line) (e) bonds.

(O2) with one of the Al capped atoms replaced by Fe. The equilibrium distance for Fe–H bond is 2.04 Å and for Al–H and Fe$_{Al}$–H is 1.45 Å. The computed adsorption energy is −3.48% more stable than the corresponding energy for the perfect alloy. We found an electron transfer of nearly 0.21e$^-$ comes from the metals to H. The DFT calculations of Fu and Painter have predicted that H dilates the Fe–Al lattice and decreases its cohesive strength when H is absorbed in Fe-rich sites [40]. Fu and Wang have studied the effect of ordering, vacancies and the mechanism underlying the hydrogen-induced embrittlement effect [41]. These authors have found hydrogen located at the tetrahedral sites with a Fe–H distance of 1.55 Å with a decrease in the Fe d charge along the Fe–H direction on Fe sites.

After H absorption the total DOS shows several small peaks (see Fig. 7) below −12 eV, which is similar to that obtained when H is located as interstitial (O2 site) at a pure cell of B2 FeAl [27]. The most important interaction of H is developed with Al. A difference with the perfect B2 FeAl is that H–metal equilibrium distances are the same (1.45 Å).

The OPDOS curves for the B2 FeAl alloy with a Fe antisite after H absorption are shown in Fig. 8. The OPDOS curves show that the Al–Al interaction is almost all bonding. The Fe–H interaction presents some antibonding peaks at −17.5 eV (see Fig. 8d), while the Al–H OP is the stronger interaction (see Fig. 8a) being 45% higher than the corresponding Fe antisite. The reported OP is much lower than that reported in FePd alloys or BCC Fe with defects [38,42].

5. Conclusions

According to our calculations the H absorption is a favorable process in the B2 Fe–Al alloy structure. H is stabilized at an octahedral interstitial site (O2) with one Al replaced by Fe.

The Al–H and Fe$_{Al}$–H distances are similar, and an electron transfer of about 0.21e$^-$ from metals to H is observed.

The electronic structure for the pure B2 Fe–Al with an Al vacancy shows a series of localized sp peaks for the Al–Al bonds and more delocalized for the Fe–Fe bonds. Considering the Fe antisite and after H absorption, the Al–Al bond is weakening 3.2% from its initial value. H locates between Fe and Al atoms as indicated in Fig. 2, so new bonds are formed: Fe–H and Al–H at expenses of the former Fe$_{Al}$–Al bond. By other hand, the Fe–Al (not antisite) bond decreases up to −41.5% after H adsorption. The Al–H interaction is developed in an interaction with Fe antisite. The Fe–Fe bond is weakened 34%, a situation that is quite different to the 70% decrease in the bond strength for pure BCC Fe when H is absorbed. It seems that Al could protect some Fe–Fe bond and this effect could be suitable to mitigate the well-known phenomena of H embrittlement.

Acknowledgments

Our work was supported by a PIP-CONICET, SGCyT-UNS and ANPCYT-PICT 2007. E.A.G., P.V.J., G.B. and A.J. are members of CONICET.

References

[1] D. Fuks, A. Struz, A. Kiv, Internat. J. Quantum Chem. 102 (2005) 606.
[2] S.F. Kettle, Physical Inorganic Chemistry: A Coordination Chemistry Approach, Oxford University Press, New York, 2000.
[3] H. Xiao, I. Baker, Acta Metall. Mater. 42 (1994) 1535.
[4] I. Baker, P. Munroe, Properties of B2 compounds, in: S. Whang, C. Liu, D. Pope, J. Stiegler (Eds.), High Temperature Aluminides and Intermetallics, TMS, Warrendale, PA, 1990.
[5] C. Vailhe, D. Farkas, Acta Mater. 45 (1997) 4463.
[6] H. Hosoda, K. Inoue, Y. Mishima, Mater. Res. Soc. Symp. Proc. 365 (1995) 437.
[7] M. Tsunekane, K. Yoshimi, K. Maruyama, Acta Mater. 56 (2008) 3162.
[8] J.P. Riviere, J. Grilhe, Acta Metall. 20 (1972) 1275.
[9] C.L. Fu, M.H. Yoo, Acta Metall. Mater. 40 (1992) 703.
[10] J. Zou, C.L. Fu, Phys. Rev. 51 (1995) 2115.
[11] S.K. Bose, V. Drchal, J. Kudrnovsky, O. Jepsen, O.K. Andersen, Phys. Rev. 55 (1997) 8184.
[12] V. Shott, M. Fähnle, Phys. Rev. 58 (1998) 14673.
[13] B.V. Reddy, P. Jena, S.C. Deevi, Intermetallics 8 (2000) 1197.
[14] B.V. Reddy, S.C. Deevi, F.A. Reuse, S.N. Khanna, Phys. Rev. B 64 (2001) 132408.
[15] B.V. Reddy, S.C. Deevi, A.C. Lilly, P. Jena, J. Phys. Cond. Matter 13 (2001) 8363.
[16] G.P. Das, B.K. Rao, P. Jena, S.C. Deevi, Phys. Rev. B 66 (2002) 184203.
[17] P. Mohn, C. Persson, P. Blaha, K. Schwarz, P. Novák, H. Eschrig, Phys. Rev. Lett. 87 (2001) 196401.
[18] D.A. Papaconstantopoulus, C. Stephen Hellberg, Phys. Rev. Lett. 89 (2002) 29701.
[19] F. Lechermann, F. Welsch, C. Elsässer, C. Ederer, M. Fähnle, J. Sanchez B. Meyer, Phys. Rev. B 65 (2002) 132104.
[20] J. Bogner, W. Steiner, M. Reissner, P. Mohn, P. Blaha, K. Schwarz, R. Krachler H. Isper, B. Sepiol, Phys. Rev. B 58 (14) (1998) 922.
[21] A. Kellou, T. Grosdidier, H. Aourag, Intermetallics 14 (2006) 142.
[22] C.T. Liu, C.L. Fu, E.P. George, G.S. Painter, ISIJ Internat. 31 (1991) 1192.
[23] B.V. Reddy, S.C. Deevi, F.A. Reuse, S.N. Khanna, Phys. Rev. B 64 (2001) 132408.
[24] Amsterdam Density Functional Package Release, Vrije Universiteit, Amsterdam, 2001.
[25] D. Becke, Phys. Rev. A 38 (1988) 3098.
[26] C. Lee, W. Yang, R.G. Parr, Phys. Rev. B 37 (1988) 785.

[27] E. González, P. Jasen, G. Brizuela, R. Nieminen, A. Juan, Phys. Status Solidi B 244 (2007) 3684.
[28] R. Podlucky, A. Neckel, Phys. Status Solidi B 95 (1979) 541.
[29] C. Blass, J. Redinger, S. Mannine, V. Honkiäki, K. Hämäläinen, P. Suortti, Phys. Rev. Lett. 75 (1995) 1984.
[30] Ch. Müller, H. Wonn, W. Blau, B. Ziesche, V.B. Krivitskii, Phys. Status Solidi B 95 (1979) 215.
[31] B.I. Min, T. Oguchi, H.J.F. Jansen, A.J. Freeman, J. Magn. Magn. Mater. 54–47 (1986) 1091.
[32] R.E. Watson, M. Weinert, Phys. Rev. B 58 (1998) 5981.
[33] D. Nguyen-Manh, D. Mayou, A. Pasturel, F. Cyrot-Lackmann, J. Phys. F 15 (1985) 1991.
[34] A.A. Ostroukhov, V.M. Floka, V.T. Cherepin, Surf. Sci. 352 (1996) 919.
[35] P.A. Schultz, J.W. Davenport, J. Alloys Compd. 197 (1993) 229.
[36] N.I. Kulikov, A.V. Postnikov, G. Borstel, J. Braun, Phys. Rev. B 59 (1999) 6824.
[37] G.A. Botton, G.Y. Guo, W.M. Temmerman, C.J. Humphreys, Phys. Rev. 54 (1996) 1682.
[38] A. Juan, R. Hoffmann, Surf. Sci. 421 (1999) 1.
[39] M. Fähnle, J. Mayer, B. Meyer, Intermetallics 7 (1999) 315.
[40] C.L. Fu, G.S. Painter, J. Mater. Res. 6 (1991) 719.
[41] C.L. Fu, X. Wang, Mat. Sci. Eng. A 239–240 (1997) 761.
[42] E.A. González, P.V. Jasen, N.J. Castellani, A. Juan, J. Phys. Chem. Solids 65 (2004) 1799.